19th Brazilian Congress of Thermal Sciences and Engineering
November 6th–10th, 2022, Bento Gonçalves - RS - Brazil

ENC-2022-0184
EXTERNAL LAMINAR BOUNDARY LAYER SIMULATIONS USING A HIGH-FIDELITY WALL-MODELING APPROACH

Eron T. V. Dauricio
Instituto Tecnológico de Aeronáutica, 12228–900, São José dos Campos, SP, Brazil
eron.tiago90@gmail.com

Carlos Junqueira-Junior
Arts et Métiers Institute of Technology, DynFluid, CNAM, HESAM University, 151 Boulevard de l'Hôpital, 75013, Paris, France
junior.junqueira@ensam.eu

Diego F. Abreu
Instituto Tecnológico de Aeronáutica, 12228–900, São José dos Campos, SP, Brazil
mecabreu@yahoo.com.br

João Luiz F. Azevedo
Instituto de Aeronáutica e Espaço, 12228–904, São José dos Campos, SP, Brazil
joaoluiz.azevedo@gmail.com

Abstract. *Accurate simulations of turbulent flows under different flow conditions are still and open challenge in the CFD community, in part due of the random nature of the turbulence phenomena, but also because of the prohibitive computational costs resulting from turbulent scale resolution requirements. In the Wall-Modeled Large Eddy Simulation (WMLES) approach, modeling of the near-wall dynamics is employed in order to alleviate such costs. However, in external boundary layer flows, the accurate simulation of the thin, pre-transition laminar boundary layer developing near the body leading edge greatly increases the computational costs, since this region is not modeled in the approach. In this work, we address this problem and propose a wall-modeling approach for this region. The new wall model is based on local self-similar solutions of the boundary layer, and is implemented in the same context of wall-stress models in the WMLES approach. An assessment of the model is performed in terms of the predicted pressure and skin friction coefficients, for an essentially incompressible, laminar flow around a NACA 0012 airfoil geometry. The results demonstrate the feasibility of the proposed wall-modeling approach, and the coefficients obtained with the model are in good agreement with the reference solution.*

Keywords: *Wall-Modeling, Wall-Modeled Large Eddy Simulation, External Laminar Flow, Boundary Layer Flow*

1. INTRODUCTION

In spite of the enormous progress, developments and improvements of computational simulations of fluid flows witnessed during the past decades, accurate simulation of turbulent flows is still an open challenge. Fully-resolved simulations of such flows demand massive computational resources due to scale resolution requirements, making it quite infeasible for practical engineering configurations. Moreover, the relationship between the larger turbulent scales and the problem boundary conditions leads to many difficulties in approaches that pursue modeling of the turbulence dynamics, since they become particular to each flow and configuration.

The Large Eddy Simulation (LES) is an approach that resolves the large, energy-containing turbulent scales, while modeling the smaller ones. Since the smaller scales tend to be more homogeneous and less dependent on boundary conditions, models employed in the LES approach are usually appropriate for a wide range of distinct flow configurations. Nonetheless, for high Reynolds number flows, the resolution needed to resolve the important near-wall dynamics imposes quite restrictive requirements on the level of mesh refinement in this region. Therefore, the computational costs become prohibitive for such cases. This situation configures the so-called "LES near-wall problem".

In order to deal with the LES near-wall problem, different solutions have been proposed, all of which incorporates

some way of modeling the effects of the near-wall motions onto the overall turbulent flow. Among these propositions is the Wall-Modeled Large Eddy Simulation (WMLES), where the inner portion of the turbulent boundary layer is modeled, while the outer portion is fully resolved. However, for external flows with high Reynolds number, the computational costs of resolving the very thin laminar boundary layer developing in the vicinity of the leading edge are still prohibitively high.

Larsson *et al.* (2016) estimated the cost of resolving the boundary layer flow along the surface of a NACA0012 airfoil. Even if the WMLES is employed, meaning that only the outer boundary layer is resolved, the number of grid points is massive near the leading edge, where the developing laminar boundary layer is very thin, being proportional to $1/\delta^2(x)$. In another study, it has been estimated that the cost of accurately solving the very thin laminar boundary layer near the leading edge of an airfoil may be 10 to 100 times higher than the cost of solving the modeled turbulent region (Slotnick *et al.*, 2014). These estimates show that, for high Reynolds number external flows, even the WMLES is still unfeasible due to high computational costs.

In this work, we propose a wall-modeling strategy for the laminar region of the boundary layer in order to alleviate the computational cost of accurately solving the thin boundary layer near the body leading edge in external flows. The laminar modeling procedure described in this work is applied in the same way as wall-stress models in the WMLES approach, since these are intended to be combined as seamlessly as possible into a single, complete flow simulation process.

2. NUMERICAL METHODOLOGY

2.1 Governing Equations

The governing equations to be solved numerically are the compressible Navier-Stokes equations, which may be written in conservation form and compact vector notation as

$$\frac{\partial \mathbf{Q}}{\partial t} + \nabla \cdot \mathbf{F}(\mathbf{Q}, \nabla \mathbf{Q}) = 0 \tag{1}$$

where $\mathbf{Q} = [\rho, \rho u_i, \rho E]^T$ is the vector of conserved variables, and $\mathbf{F}$ is the flux vector, given by $\mathbf{F} = \mathbf{F}^e - \mathbf{F}^v$, with the superscripts e and v indicating advective, or Euler, and viscous fluxes, respectively. These may be further written as

$$\mathbf{F}_i^e = \begin{bmatrix} \rho u_i \\ \rho u_1 u_i + \delta_{1i} p \\ \rho u_2 u_i + \delta_{2i} p \\ \rho u_3 u_i + \delta_{3i} p \\ (\rho E + p)\, u_i \end{bmatrix}, \quad \mathbf{F}_i^v = \begin{bmatrix} 0 \\ \tau_{1i} \\ \tau_{2i} \\ \tau_{3i} \\ u_j \tau_{ij} - q_i \end{bmatrix}, \quad i = 1, 2, 3 \tag{2}$$

In the above equations, ρ is the density, u_i are the components of the velocity vector, and ρE is the total energy per unit volume. In order to obtain closure of the system of equations, the total energy per unit volume is written in terms of the thermodynamic pressure using the thermal and caloric equations of state for an ideal gas, that is, $p = \rho R T$ and $e = c_v T$, respectively. Then, one can write

$$\rho E = \rho e + \frac{1}{2}\rho u_i u_i = \frac{p}{(\gamma - 1)} + \frac{1}{2}\rho u_i u_i$$

where e is the internal energy per unit mass, and γ and R are the ratio and the difference between specific heats, respectively.

The viscous stress tensor, τ_{ij}, may be written as

$$\tau_{ij} = \mu \left(\frac{\partial u_i}{\partial x_j} + \frac{\partial u_j}{\partial x_i} \right) + \lambda \left(\frac{\partial u_k}{\partial x_k} \right) \delta_{ij} \tag{3}$$

where μ and λ are the dynamic and the second coefficients of viscosity, related by Stokes' hypothesis as $\lambda = -\frac{2}{3}\mu$. The heat flux vector, q_i, in Eq. (2) is given by

$$q_i = -k \frac{\partial T}{\partial x_i}$$

with k as the thermal conductivity coefficient.

2.2 Numerical Method

In this work, Eq. (1) is numerically solved through a nodal implementation of the discontinuous Galerkin (DG) scheme with split formulations for the inviscid fluxes. We start by discretizing the physical domain, Ω, into K non-overlapping

elements, Ω_k, such that

$$\Omega \approx \Omega_h \equiv \bigcup_{k=1}^{K} \Omega_k, \qquad \bigcap_{k=1}^{K} \Omega_k = \emptyset$$

where Ω_h is the computational domain.

The elements in physical domain are then mapped onto a standard element, Ω_{st}, where each shape in physical domain have a corresponding shape in the standard domain. Although the shape of the discretizing elements are arbitrary, in this work we use only hexahedral elements, primarily due to computational efficiency and ease of implementation. For this shape, the standard element is defined by $\Omega_{st} = [-1, 1]^3$. Applying this mapping to Eq. (1) results in

$$\boldsymbol{J}\frac{\partial \boldsymbol{Q}}{\partial t} + \nabla_\xi \cdot \boldsymbol{\mathcal{F}} \equiv \boldsymbol{J}\frac{\partial \boldsymbol{Q}}{\partial t} + \nabla_\xi \cdot \left(\boldsymbol{e}^\xi \cdot \mathbf{F}\right) = 0 \tag{4}$$

where ∇_ξ is the divergence with respect to the standard element coordinates, $\boldsymbol{\xi} = (\xi, \eta, \zeta)$, $\boldsymbol{J} = |\partial \boldsymbol{x}/\partial \boldsymbol{\xi}|$ is the Jacobian of the coordinate transformation, $\boldsymbol{e}^\xi$ is the contravariant basis vector, and $\boldsymbol{\mathcal{F}} = \boldsymbol{e}^\xi \cdot \mathbf{F}$ the contravariant flux vector.

For the nodal implementation of the discontinuous Galerkin scheme, the solution within each element, in standard coordinates, is approximated by a polynomial interpolation given by

$$\boldsymbol{Q} \approx \boldsymbol{Q}_h(\boldsymbol{\xi}) = \sum_{p,q,r=0}^{N} \boldsymbol{Q}_h(\xi_p, \eta_q, \zeta_r, t)\phi_{pqr}(\boldsymbol{\xi}) \tag{5}$$

where ϕ_{pqr} is the interpolating polynomial. For hexahedral elements, this polynomial is given by a tensor product of 1-D Lagrange polynomials, that is,

$$\phi_{pqr}(\boldsymbol{\xi}) = \ell_p(\xi)\ell_q(\eta)\ell_r(\zeta), \qquad \ell_p = \prod_{\substack{i=0 \\ i\neq p}}^{N_p} \frac{\xi - \xi_i}{\xi_p - \xi_i}$$

with equivalent definitions for the other directions.

In the DG formulation, the residual of the approximation, obtained by substitution of Eq. (5) into Eq. (4), is required to be orthogonal to a test function, ψ, where the space of this test function is the same as the space spanned by the trial, or solution function. This leads to the following formulation

$$\int_{\Omega_{st}} J\frac{\partial \boldsymbol{Q}_h}{\partial t}\psi d\boldsymbol{\xi} + \int_{\Omega_{st}} \left(\nabla_\xi \cdot \boldsymbol{\mathcal{F}}^e\right)\psi d\boldsymbol{\xi} + \int_{\partial\Omega_{st}} \left(\boldsymbol{\mathcal{F}}^{e,\star} - \boldsymbol{\mathcal{F}}^e\right)\psi d\boldsymbol{S}_\xi - \int_{\Omega_{st}} \left(\nabla_\xi \cdot \boldsymbol{\mathcal{F}}^v\right)\psi d\boldsymbol{\xi} = 0, \tag{6}$$

where $\partial\Omega_{st}$ defines the boundary of the element, and $\boldsymbol{\mathcal{F}}^{e,\star}$ is a numerical flux function defined on this boundary. The formulation in Eq. (6) is obtained after integration by parts of the second term of Eq. (4) two times, and is called the strong formulation. The weak formulation is obtained when integration by parts is done only once. The integrals in Eq. (6) are carried out through Gaussian quadratures, where the details may be consulted in Hindenlang *et al.* (2012).

As mentioned above, a split formulation of the inviscid fluxes, $\boldsymbol{\mathcal{F}}^e$, is implemented in order to enhance stability of the method, especially for higher order interpolations. The details of this formulation are not described here due to brevity, but may be consulted in the comprehensive exposition of Gassner *et al.* (2016). The specific split form of the fluxes employed throughout the simulations in this work is that of Pirozzoli (2011). An approximate Riemann solver, namely the Roe solver with an entropy fix (Toro, 2009), is used to obtain the numerical flux $\boldsymbol{\mathcal{F}}^{e,\star}$ on the element boundaries.

Since weak variational formulations using discontinuous function spaces are not suitable for directly discretizing higher order derivatives, as those appearing in the divergence term of the viscous fluxes in Eq. (4) through the viscous stress tensor, Eq. (3), a mixed formulation must be used for these terms. In this work, we make use of the lifting scheme of Bassi and Rebay (2000).

The semidiscrete equations obtained after full discretization of Eq. (6) according to the aforementioned methods are advanced in time using the five stage, fourth-order, low-storage Runge-Kutta scheme of Carpenter and Kennedy (1994). This work uses the computational implementation of the FLEXI software (Krais *et al.*, 2021) in order to apply the numerical scheme and discretization methods just described.

3. WALL MODEL FOR LAMINAR BOUNDARY LAYERS

One of the remaining challenges in WMLES simulations is that of external flows with high Reynolds numbers. In such cases, the laminar boundary layer developing near the body leading edge is very thin, and the grid resolution required to resolve such thin region leads to a computational cost that is prohibitively high.

In this work, we propose a modeling strategy for laminar boundary layers in external flows in order to alleviate the resolution requirements needed to resolve this portion of the boundary layer in high Reynolds number flows. As such, the model presented herein seeks to calculate a wall-shear stress for boundary condition imposition, and it is argued that this condition – with the no-transpiration condition at the wall – is sufficient to recover the skin friction and pressure coefficients along the wall. The implementation of the wall-modeling procedure is done in the same manner as that for wall-stress models in the WMLES approach. This section describes the reasoning behind the model and presents its formulation, whereas the next section contains an assessment of the feasibility of the model in the aforementioned context.

The basic underlying assumption of our model is that the dynamics of the boundary layer along the wall may be given according to locally self-similar solutions. More specifically, it is assumed that at each point along the wall-tangent direction, there exists a similarity solution from the general Falkner-Skan family satisfying the boundary layer dynamics. Hence, at each point along this direction, we solve for a local similarity solution given by

$$\frac{d^3 f}{d\varepsilon^3} + \alpha f \frac{d^2 f}{d\varepsilon^2} + \beta \left[1 - \left(\frac{df}{d\varepsilon} \right)^2 \right] = 0 \tag{7}$$

with the boundary conditions

$$\varepsilon = 0: \qquad f = 0, \tag{8a}$$

$$\frac{df}{d\varepsilon} = 0, \tag{8b}$$

$$\varepsilon \to \infty: \qquad \frac{df}{d\varepsilon} = 1, \tag{8c}$$

where α and β are constant parameters, and ε is the similarity variable, written as

$$\varepsilon = \frac{y}{\lambda(x_s)}$$

with $\lambda(x_s)$ a function to be defined, and x_s the distance along the surface.

In the above ordinary differential equation, the function $f(\varepsilon)$ defines the velocity profile within the boundary layer through its first derivative,

$$\frac{df}{d\varepsilon} = \frac{u}{U_e}, \tag{9}$$

where u is the velocity within the boundary layer in the x_s direction, and U_e is the outer flow velocity, that is, the velocity at the edge of the boundary layer (Currie, 2012), which is assumed to be a function of x_s only. In boundary layer theory, this is the velocity that would be obtained for the solution in the limit of infinite Reynolds number, represented by the Euler equations.

The constant parameters α and β in Eq. (7) may be written as

$$\frac{\lambda}{\nu} \frac{d}{dx_s} (U_e \lambda) = \alpha, \tag{10a}$$

$$\frac{\lambda^2}{\nu} \frac{dU_e}{dx_s} = \beta, \tag{10b}$$

where ν is the kinematic viscosity. Thus, it can be seen that these two parameters define both the outer flow velocity, U_e, and the function $\lambda(x_s)$. Therefore, they completely define the problem to be solved. If we set $\alpha = 1$, then, the corresponding similarity variable is

$$\varepsilon = y \sqrt{\frac{1}{2-\beta} \frac{U_e}{\nu x_s}}, \tag{11}$$

and the outer flow velocity is

$$U_e(x_s) = c x_s^{\frac{\beta}{2-\beta}}, \tag{12}$$

which may be identified as the velocity of a potential flow over a wedge of half angle $\pi\beta/2$ (Currie, 2012).

In the solution process of Eq. (7), we seek a value of $d^2 f/d\varepsilon^2$ at $\varepsilon = 0$ that satisfies the boundary condition at $\varepsilon \to \infty$, Eq. (8c). This value is then used to calculate the wall-shear stress, which, for $\alpha = 1$, may be written as

$$\tau_w = \mu \sqrt{\frac{1}{2-\beta} \frac{U_e^3}{\nu x_s}} \left. \frac{d^2 f}{d\varepsilon^2} \right|_{\varepsilon=0}, \tag{13}$$

where the definitions in Eqs. (9) and (11) are used to arrive at this final form. This wall-shear stress is subsequently used to impose the boundary condition at the wall.

Following the wall-modeling procedure in the WMLES approach (Larsson *et al.*, 2016), the outer flow velocity, U_e, appearing in the equation for the wall-shear stress above, is taken from the solution farther away from the wall, at the wall-model height, h_{wm}. It is then left to determine the parameter β defining the problem to be solved in Eq. (7), thus obtaining the value of $d^2f/d\varepsilon^2$ at $\varepsilon = 0$.

In order to determine the constant parameter β, we remind that the basic assumption of the model is that the boundary layer dynamics locally satisfies a solution of Eq. (7). When $\alpha = 1$, the problem represented in Eq. (7) is that of the flow over a wedge. Thus, we assume that at each location along the body surface, the dynamics of the fluid particles are similar to those in the flow over a wedge with a half angle related to the geometric angle between the surface wall-tangent and the streamwise directions. With these assumptions, we define β as

$$\beta = \kappa - |\kappa| \left[1 - \chi\left(\frac{x}{c}, Re_c\right)\right] \tag{14}$$

where κ is defined such that $\pi\kappa/2$ is the geometric angle between the wall-tangent and streamwise directions, as illustrated in Fig. 1, and, hence, may be computed as

$$\kappa = \frac{2}{\pi} \cos^{-1}\left(\hat{\boldsymbol{t}} \cdot \hat{\boldsymbol{s}}\right), \tag{15}$$

with $\hat{\boldsymbol{t}}$ as the unit wall-tangent vector, and $\hat{\boldsymbol{s}}$ a unit vector in the streamwise direction.

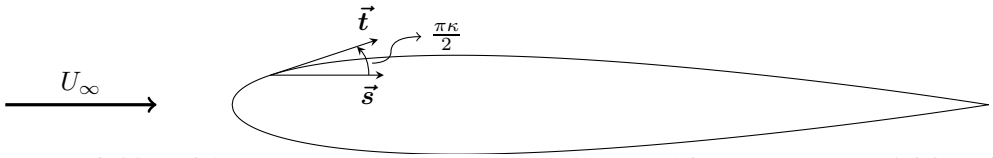

Figure 1: Definition of the geometry-related parameter κ, illustrated for a NACA 0012 airfoil surface.

In Eq. (14), χ is a correction function used to adjust the angle κ obtained solely from geometric considerations. This correction is justified on physical grounds. If $\beta = \kappa$ is used directly, the solution obtained from Eq. (7) is that of a flow that accelerates as much as the inviscid flow over a wedge of half angle $\pi\kappa/2$. In this case, the velocity gradient within the boundary layer must be higher than that obtained for a viscous flow over the same wedge and, consequently, the computed wall-shear stress is overpredicted. The boundary layer is actually a dissipation of this gradient through viscosity, thus reducing the wall-shear stress when compared to the inviscid flow case. Therefore, since $d^2f/d\varepsilon^2$ is directly proportional to the constant parameter defining the problem (Schlichting and Gersten, 2000), a reduction in the wall-shear stress as computed from Eq. (13) is achieved by decreasing the geometric angle κ in the definition of the parameter β.

Another way to justify this angle correction is to see the practical effect of the boundary layer as an obstruction for the flow field, acting to decrease the acceleration along the wedge. This same decreased acceleration may be obtained for the flow in a wedge with a lower half angle. Since the reasoning above applies regardless of whether κ is positive or negative, the adjustment is written in terms of $|\kappa|$.

From the rationale above, which accounts for the effects of the viscous boundary layer in the definition of the parameter β, it is intuitive that the correction function in Eq. (14) must be related to a Reynolds number and a characteristic length along the surface. Viscous effects become less pronounced the higher the Reynolds number, while the boundary layer grows thicker the further downstream along the surface. Since this work deals with flows around airfoils, we choose the chord Reynolds number, Re_c, and the downstream distance relative to the chord, x/c, when defining the correction function, and write it as

$$\chi\left(\frac{x}{c}, Re_c\right) = \frac{1 - \left(\sqrt{x/c}\right) e^{-ARe_c}}{1 + e^{-ARe_c}} \tag{16}$$

where A is a coefficient, and the chord Reynolds number is given by

$$Re_c = \frac{U_\infty c}{\nu},$$

with U_∞ the free-stream velocity magnitude. Notice that x in the equation above is the distance in the streamwise direction, as opposed to the distance along the surface, x_s, used in the boundary layer equations.

The function in Eq. (16) has the following desired property,

$$Re_c \to \infty, \quad \chi \to 1,$$

that is, in the limit of infinite Reynolds number, no adjustment is made to the geometric angle κ, and the solution obtained by solving Eq. (7) refers to that of a flow accelerating as much as the inviscid flow over a wedge of half angle $\pi\kappa/2$, as desired. In addition, we have that

$$Re_c \to -\infty, \quad \chi \to -\sqrt{x/c},$$

and, although the above limit is not physically possible, this property means that, for a given chord Reynolds number, as $\sqrt{x/c}$ grows larger, and hence the boundary layer thickens, the correction function χ decreases, such that the adjustment in Eq. (14) is more pronounced. The coefficient A is a free constant parameter to fine tune the angle correction. Preliminary parametric studies indicate that a sufficiently good value for this parameter is $A = 2.63 \times 10^{-5}$, and this is used throughout this work.

After the definition of the parameter β for each location along the surface, Eq. (7) is solved using the iterative procedure described in Zhang and Chen (2009). The method employs a free boundary formulation, and uses a shooting method to transform the initial boundary-value problem into a set of initial-value problems, which are solved using standard Runge-Kutta methods. The solution using this iterative method directly outputs the quantity of interest $d^2 f/d\varepsilon^2$ at $\varepsilon = 0$.

4. RESULTS AND DISCUSSION

This section presents the results obtained for the simulations of laminar flows around a NACA 0012 airfoil at zero angle of attack using the wall model described in Sec. 3. Since the model is only intended to be used in laminar flow regions, the test cases that constitute the validation process must exhibit relatively low Reynolds number in order to prevent transition to turbulence. At such low Reynolds numbers, it is difficult to sustain an entirely attached flow against an adverse pressure gradient, and separation of the boundary layer is likely to take place at some position downstream of the leading edge.

The validation of the wall model is done for a flow around a NACA 0012 geometry, even though separation is only absent for very low Reynolds numbers in this case. In order to keep the separation region as mild and as further away from the leading edge as possible, the current wall modeling strategy is validated primarily in a flow with a chord Reynolds number of $Re_c = 4.5 \times 10^3$, which remains laminar in its entirety. The Mach number for every simulation in this work is $M_\infty \approx 0.2$, and thus the flow is essentially incompressible. A fully resolved simulation is performed, under the same flow conditions and with a sufficiently fine mesh – capable of correctly capturing the boundary layer dynamics – in a wall-resolved configuration, to provide the benchmark solution for results comparisons.

The performance of the model is assessed in terms of the predicted pressure coefficient, C_p, and skin friction coefficient, C_f, along the surface. A mesh with $96 \times 44 \times 1$ hexahedral elements is used, where the first number indicates the elements in the direction along the surface, whereas the second indicates the elements in the wall-normal direction. The distribution of the elements along the surface is uniform, meaning that Δx_s is constant throughout. It should be noted that, although the flow is two-dimensional, a full, three-dimensional simulation is performed, where only a single element is generated in the spanwise direction. Figure 2 illustrates this mesh.

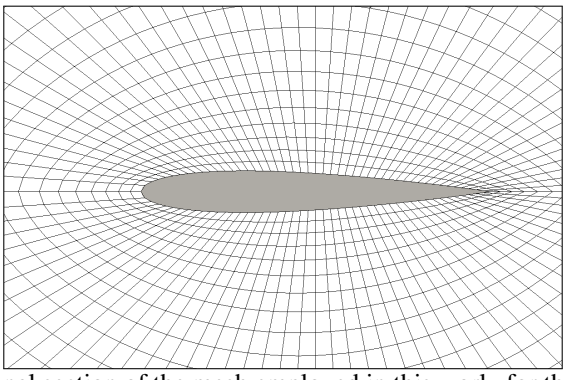

Figure 2: Two-dimensional section of the mesh employed in this work, for the region near the airfoil.

In addition, the effects of the wall-model height, h_{wm}, the main parameter of the wall-modeling procedure, are also investigated. We assume a linear growth of the exchange location where the outer flow velocity is extracted, starting from $x/c = 0$ and increasing along the streamwise direction, x. Three different growth rates are tested, as described in Table 1 and shown in Fig. 3, where it should be noted that the wall model height, h_{wm}, is a distance from the wall in the wall-normal direction. The boundary layer edge, extracted from the fully resolved simulation, is shown for comparison.

In the assessment of the model, the pressure and skin friction coefficients are plotted for both the upper (suction) and lower (pressure) surfaces of the airfoil, with filled symbols for the former and open symbols for the latter. As expected for a symmetric airfoil at zero angle of attack, the coefficients along the surface are exactly the same for both upper and lower surface and, hence, they are superimposed in the plots below.

Table 1: Shape and growth rate of the wall model height, h_{wm}, tested in the simulations.

Growth type	Growth rate	$h_{wm}(x)/c$
Linear	Low	$0.04\,x/c + 0.01$
	Medium	$0.08\,x/c + 0.01$
	High	$0.11\,x/c + 0.01$

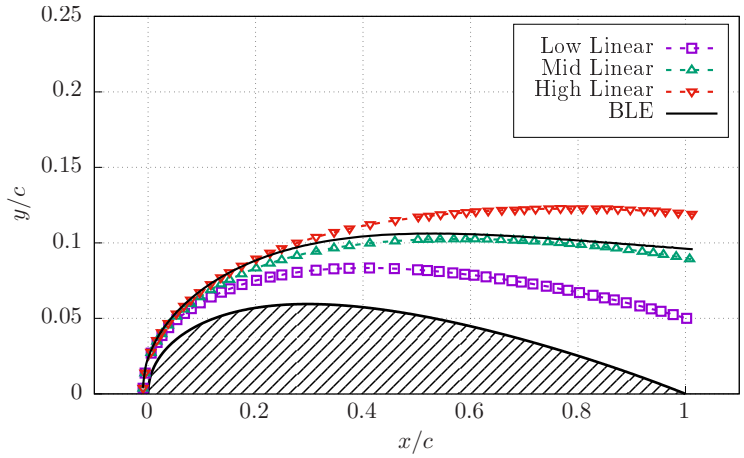

Figure 3: Wall model heights with linear growth along the surface, for different growth rates. The boundary layer edge (BLE) obtained from a fully resolved simulation is also shown.

The results are compared to those obtained from a fully resolved simulation, using a mesh sufficiently fine to resolve for all the viscous dynamics of the flow, with no wall modeling. In all the plots presenting the solutions, points along the lines are used only for distinguishing different results, and are not representative of grid points. The accuracy of the proposed wall model is first investigated using the wall model height with medium growth rate – see Fig. 3. This exchange location is chosen for the investigation because it is the one that more closely resembles the actual edge of the boundary layer. The results obtained for this simulation are shown in Fig. 4.

The pressure and skin friction coefficients predicted by the model are very close to the reference solution, both qualitatively and quantitatively, despite the quite restrictive basic assumption of the model. Near the leading edge, it is seen that the solution obtained with the wall model accelerates slightly more than the reference viscous solution, resulting in a lower pressure in this region. Moreover, the deceleration in the rear portion of the airfoil is also more pronounced, resulting in a higher pressure for the results obtained with the wall model. This is a direct consequence of imposing a lower wall-shear stress in the acceleration region, and a higher wall-shear stress in the deceleration region, when compared to the fully resolved simulation, as is evident from the results for the skin friction coefficient. This should not be seen as a flaw of the model, since the imposed wall-shear stress may be adjusted by changing the parameters of the model in the correction function χ – cf. Eq. (14).

The behavior of the skin friction coefficient very near the leading edge, as predicted by the wall model solution, is far from the one obtained for the fully resolved simulation. It may be seen that the skin friction coefficient is very high for $x/c \approx 0$, followed by a narrow, negative skin friction region, from which it catches up with the expected behavior, qualitatively. From Eq. (13), defining the wall-shear stress to be imposed as the boundary condition, we see that the leading edge, $x/c = 0$, is a singularity point. Thus, at this location, the wall-shear stress is ill-defined, and the wall model needs special treatment. The effect of imposing an extremely high wall-shear stress at the leading edge, when no special treatment of this location is employed, is that the flow separates, resulting in a very narrow region of reverse flow, from which it recovers shortly after, given the favorable pressure gradient.

For the solutions obtained with the wall-modeling approach, the cumulative skin friction along the surface – that is, the integrated force – is not sufficient to cause boundary layer separation. In the fully resolved simulation, however, separation occurs when the flow is approaching the trailing edge, at approximately $x/c \approx 0.92$. In a slightly higher Reynolds number flow, $Re_c = 5 \times 10^3$, separation is also present in the simulations of Swanson and Langer (2016), and it takes place at $x/c \approx 0.8$. It should be noted, however, that the simulations in Swanson and Langer (2016) concern compressible flows, with a Mach number of $M_\infty = 0.5$.

The solution for the pressure coefficient, C_p, exhibits wiggles near the leading edge. These are spurious oscillations that appear due to the fact that the mesh is too coarse to accurately represent the curvature of the airfoil geometry (Bassi and Rebay, 1997). Such spurious oscillations appear even in the solution for the fully resolved simulation, although with remarkably lower amplitude. From the results shown in Fig. 4, the feasibility of the model is demonstrated. The

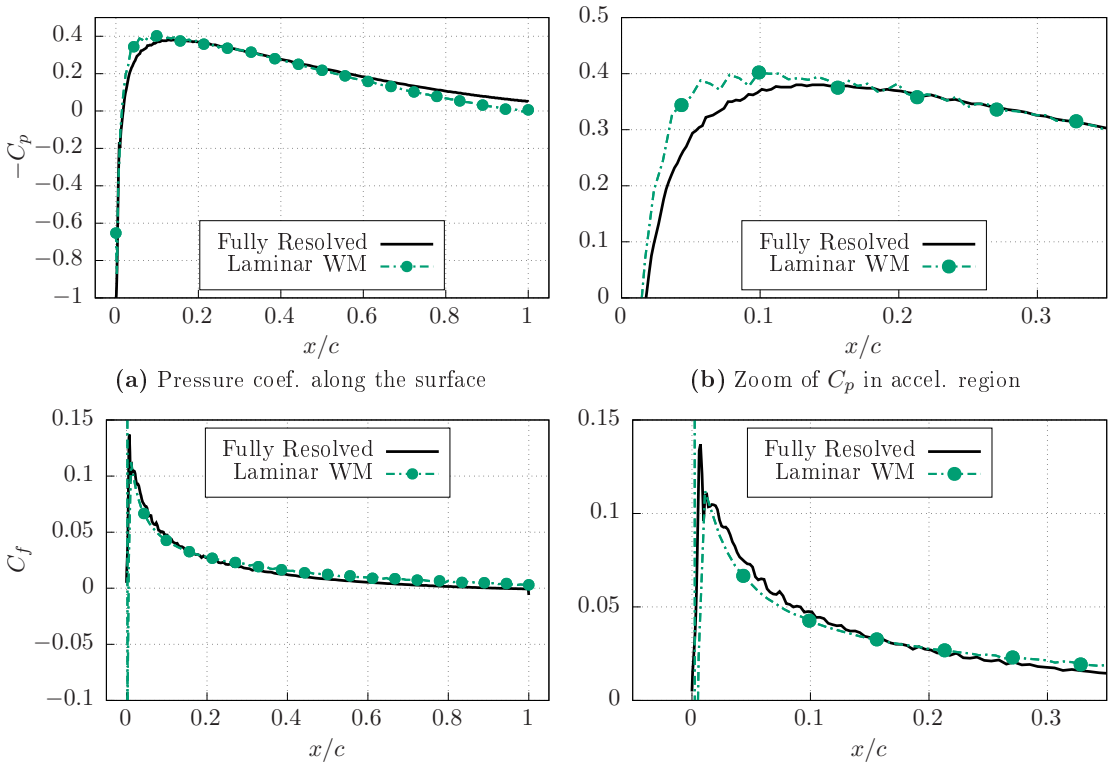

(a) Pressure coef. along the surface

(b) Zoom of C_p in accel. region

(c) Skin friction coef. along the surface

(d) Zoom of C_f in accel. region

Figure 4: Solutions of pressure and skin friction coefficients for the proposed laminar wall model, using the wall model height with medium growth rate. Filled symbols: suction side; open symbols: pressure side. Symbols are superimposed.

discrepancies observed may be adjusted by parameter fine-tuning, and the behavior of the skin friction coefficient in the vicinity of the leading edge may be corrected by an appropriate treatment of the computed wall-shear stress at the singularity point, $x/c = 0$.

A very important aspect of every wall model employed in the context of wall-stress models is the effect of changes in the exchange location, h_{wm}, onto the predicted results. This parameter is usually defined in terms of the boundary layer thickness, δ, or, similarly, the ratio h_{wm}/δ. Since this quantity is not know prior to the simulation, a model that is insensitive to the exchange location is less restrictive in terms of the initial definition of h_{wm}.

Figure 5 shows the results obtained for the simulations using the three previously described wall model heights, with low, medium and high growth rates along the streamwise direction. These simulations are all performed in the same mesh, depicted in Fig. 2, such that any influence regarding mesh refinement or element distribution is isolated.

Similar to the results shown in Fig. 4 for the medium growth rate of the wall model height, all the results shown in Fig. 5 are in very good agreement with the reference solution, especially from a qualitative point of view. When the solutions for the distinct wall model heights are compared to each other, it may be seen that only the results obtained with the smallest growth rate is distinguishable from the others. Moreover, differences are only seen for the pressure coefficient. We note that the wall model height for the lower growth rate is too close to the wall and, as a consequence, the probed velocity, U_e, is not representative of the outer flow velocity. For both medium and high growth rates, on the other hand, the results are essentially the same, since the wall model height in these cases are farther from the wall, and more closely matches the boundary layer edge.

Considering that the results are very close to each other, the same behavior discussed for the previous solution is observed here. The skin friction coefficient is underpredicted in the region near the leading edge, whilst being overpredicted at the rear portion of the airfoil. Consequently, the pressure is slightly lower near the leading edge due to an excess acceleration for the results using the wall modeling procedure. None of the solutions exhibit boundary layer separation near the trailing edge, however, as is expected from the behavior in the reference simulation.

Spurious oscillations appear in the solutions of the pressure coefficient for every distinct wall model height tested, as briefly discussed for the results shown in Fig. 4. This is another evidence that such wiggles are a consequence of insufficient discrete representation of the airfoil curvature, and is not related to the proposed wall model. Another aspect of the results is that the wall-model height, h_{wm}, have very little effect on the predicted pressure coefficient. This is to be expected, since the pressure distribution at the wall is imposed from the outer flow solution and, therefore, viscous effects have little influence for fully attached flows. Nonetheless, the same behavior is observed for the predicted skin friction coefficient, where the influence of the wall model height is mild. As mentioned previously, low sensitiveness to

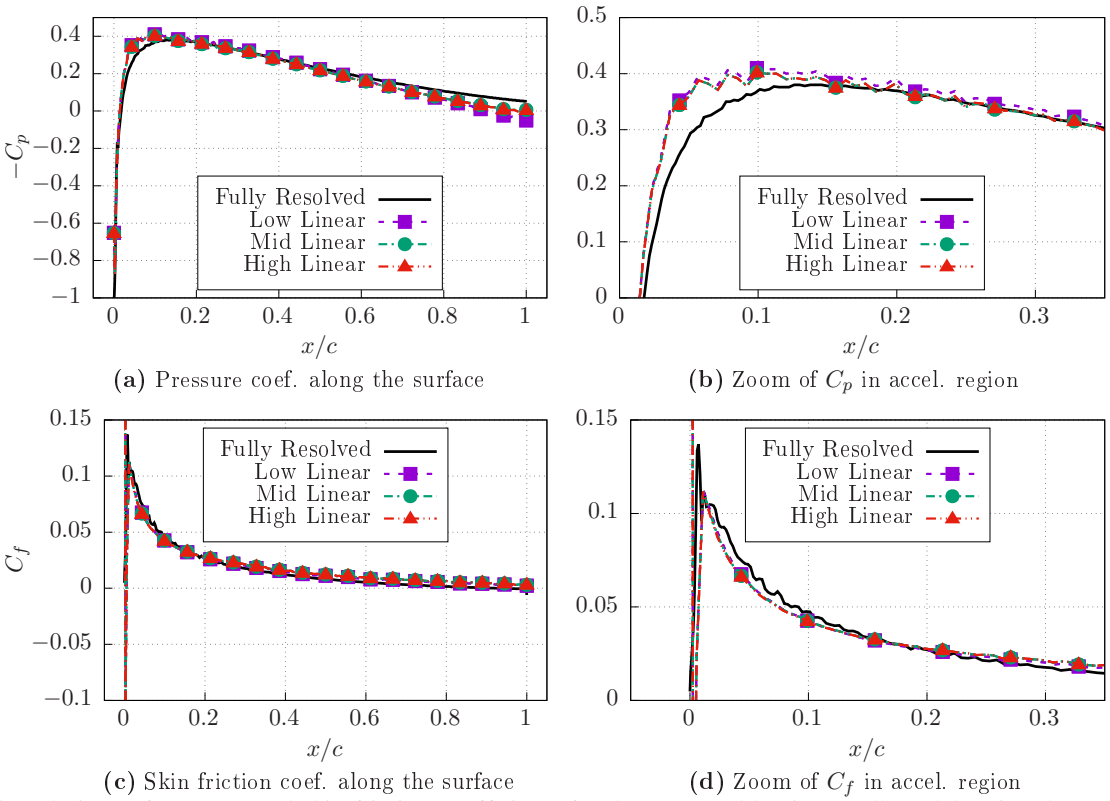

(a) Pressure coef. along the surface

(b) Zoom of C_p in accel. region

(c) Skin friction coef. along the surface

(d) Zoom of C_f in accel. region

Figure 5: Solutions of pressure and skin friction coefficients for the proposed laminar wall model, using the wall model height with medium growth rate. Filled symbols: suction side; open symbols: pressure side. Symbols are superimposed.

the exchange location is an important feature of the wall model, where restrictions on the correct definition of an initial wall model height, h_{wm}, are relaxed.

5. CLOSING REMARKS

This work proposes a wall-modeling approach for simulations of external laminar boundary layers, based on local self-similar solutions. The wall model uses information from the numerical solution farther away from the wall, combined with local self-similar solutions of the Falkner-Skan family in order to provide a wall-shear stress that is subsequently imposed as a boundary condition. The proposed wall model is validated on simulations of an essentially incompressible, low Reynolds number flow, with $Re_c = 4.5 \times 10^3$ and $M_\infty \approx 0.2$, where the boundary layer flow remains laminar in its entirety. The results show the feasibility of the proposed model for essentially incompressible, low Reynolds number flows. The solutions obtained with the wall model exhibits excellent behavior for both the pressure and skin friction coefficients, following very closely the solutions obtained in a fully resolved simulation without wall modeling.

The wall model as proposed in Sec. 3, with the constant parameter β as defined by Eqs. (14)-(16), computes a wall-shear stress that is too low in the acceleration region, and too high in the deceleration region. Consequently, the predicted pressure distribution along the surface is too low in the acceleration region, and too high in the deceleration region. One way to adjust the computed wall-shear stress to match that obtained in a fully resolved solution is by a corresponding adjustment of the correction function, χ, through parameter fine tuning.

An important feature of the laminar wall model is that the solutions for the pressure and skin friction coefficients are quite insensitive to the wall model height, h_{wm}. Hence, the limitations on the initial definition of the exchange location are relaxed, since locations that are not strictly matching the boundary layer edge provide reasonably accurate results. Although spurious oscillations in the pressure distribution along the surface may be seen for every result presented in this work, we claim that such wiggles are a consequence of the mesh coarseness and its failure to accurately represent the curved geometry of the airfoil in the acceleration region. The laminar wall model, as presented in this work, may be readily combined with a turbulent wall model in the context of wall-stress models in WMLES solutions, in order to perform a simulation of the complete developing boundary layer in external flows with reasonable computational costs for all regions and regimes of the boundary layer.

6. ACKNOWLEDGEMENTS

The authors acknowledge the support for the present research provided by Conselho Nacional de Desenvolvimento Científico e Tecnológico, CNPq, under the Research Grant No. 309985/2013-7. The work is also supported by the

computational resources from the Center for Mathematical Sciences Applied to Industry, CeMEAI, funded by Fundação de Amparo à Pesquisa do Estado de São Paulo, FAPESP, under the Research Grant No. 2013/07375-0. The authors further acknowledge the National Laboratory for Scientific Computing (LNCC/MCTI, Brazil) for providing HPC resources of the SDumont supercomputer. This work was also granted access to the HPC resources of IDRIS under the allocation 2021-A0112A12067 made by GENCI. The first author acknowledges the financial support in the form of a doctoral scholarship from FAPESP, under the Grant No. 2018/05524-1. The third author acknowledges authorization by his employer, Embraer S.A., which has allowed his participation in the present research effort. Additional support to the fourth author under the FAPESP Research Grant No. 2013/07375-0 is also gratefully acknowledged.

7. REFERENCES

Bassi, F. and Rebay, S., 1997. "High-order accurate discontinuous finite element solution of the 2D Euler equations". *Journal of Computational Physics*, Vol. 138, No. 2, pp. 251–285.

Bassi, F. and Rebay, S., 2000. "A high-order discontinuous Galerkin method for compressible turbulent flows". In B. Cockburn, G.E. Karniadakis and C.W. Shu, eds., *Discontinuous Galerkin Methods: Theory, Computation and Applications*, Springer-Verlag, Lecture Notes in Computational Science and Engineering, pp. 77–88.

Bose, S.T. and Park, G.I., 2018. "Wall-modeled large-eddy simulation for complex turbulent flows". *Annual Review of Fluid Mechanics*, Vol. 50, pp. 535–561.

Carpenter, M.H. and Kennedy, C.A., 1994. "Fourth-order 2n-storage Runge-Kutta schemes". NASA-TM-109112, NASA Langley Research Center.

Choi, H. and Moin, P., 2012. "Grid-point requirements for large eddy simulation: Chapman's estimates revisited". *Physics of Fluids*, Vol. 24, No. 1, p. 011702.

Currie, I.G., 2012. *Fundamental Mechanics of Fluids*. CRC Press, Boca Raton, 4th edition.

Deardorff, J.W., 1970. "A numerical study of three-dimensional turbulent channel flow at large reynolds numbers". *Journal of Fluid Mechanics*, Vol. 41, No. 2, pp. 453–480.

Gassner, G.J., Winters, A.R. and Kopriva, D.A., 2016. "Split form nodal discontinuous Galerkin schemes with summation-by-parts property for the compressible Euler equations". *Journal of Computational Physics*, Vol. 327, pp. 39–66.

Hindenlang, F., Gassner, G.J., Altmann, C., Beck, A., Staudenmaier, M. and Munz, C.D., 2012. "Explicit discontinuous Galerkin methods for unsteady problems". *Computers and Fluids*, Vol. 61, pp. 86–93.

Hoyas, S. and Jiménez, J., 2006. "Scaling of the velocity fluctuations in turbulent channels up to $Re_\tau = 2003$". *Physics of Fluids*, Vol. 18, No. 1, p. 011702.

Krais, N., Beck, A., Bolemann, T., Frank, H., Flad, D., Gassner, G., Hindenlang, F., Hoffmann, M., Kuhn, T., Sonntag, M. and Munz, C.D., 2021. "FLEXI: A high order discontinuous galerkin framework for hyperbolic–parabolic conservation laws". *Computers & Mathematics with Applications*, Vol. 81, No. 1, pp. 186–219. doi:https://doi.org/10.1016/j.camwa.2020.05.004.

Larsson, J., Kawai, S., Bodart, J. and Bermejo-Moreno, J., 2016. "Large eddy simulation with modeled wall-stress: Recent progress and future directions". *Mechanical Engineering Reviews*, Bulletin of the JSME, Vol. 3, No. 1, pp. 15–00418.

Piomelli, U. and Balaras, E., 2002. "Wall-layer models for large-eddy simulation". *Annual Review of Fluid Mechanics*, Vol. 34, pp. 349–374.

Pirozzoli, S., 2011. "Numerical methods for high-speed flows". *Annual Review of Fluid Mechanics*, Vol. 43, pp. 163–194.

Pope, S.B., 2000. *Turbulent Flows*. Cambridge University Press. 771 p.

Schiavo, L.A.C.A., Wolf, W.R. and Azevedo, J.L.F., 2017. "Turbulent kinetic energy budgets in wall bounded flows with pressure gradients and separation". *Physics of Fluids*, Vol. 29, No. 11, p. 115108. doi:10.1063/1.4992793.

Schlichting, H. and Gersten, K., 2000. *Boundary-Layer Theory*. Springer-Verlag, 8th edition.

Schumann, U., 1975. "Subgrid scale model for finite difference simulations of turbulent flows in plane channels and annuli". *Journal of Computational Physics*, Vol. 18, No. 4, pp. 376–404.

Slotnick, J., Khodadoust, A., Alonso, J., Darmofal, D., Gropp, W., Lurie, E. and Mavriplis, D., 2014. "CFD Vision 2030 study: A path to revolutionary computational aerosciences". NASA/CR-2014-218178, NASA. https://ntrs.nasa.gov/citations/20140003093.

Spalart, P.R., 2009. "Detached-eddy simulation". *Annual Review of Fluid Mechanics*, Vol. 41, No. 1, pp. 181–202. doi:10.1146/annurev.fluid.010908.165130.

Swanson, R.C. and Langer, S., 2016. "Comparison of NACA 0012 laminar flow solutions: Structured and unstructured grid methods". NASA/TM-2016-219003, NASA. https://ntrs.nasa.gov/citations/20160003623.

Toro, E.F., 2009. *Riemann Solvers and Numerical Methods for Fluid Dynamics*. Springer-Verlag, 3rd edition.

Zhang, J. and Chen, B., 2009. "An iterative method for solving the Falkner–Skan equation". *Applied Mathematics and Computation*, Vol. 210, No. 1, pp. 215–222. ISSN 0096-3003. doi:https://doi.org/10.1016/j.amc.2008.12.079.

8. RESPONSIBILITY NOTICE

The authors are solely responsible for the printed material included in this paper.